Calculations on charge state and energy loss of argon ions in partially and fully ionized carbon plasmas

Manuel D. Barriga-Carrasco,[1] David Casas,[1,2] and Roberto Morales[1]
[1]*E.T.S.I. Industriales, Universidad de Castilla-La Mancha, E-13071 Ciudad Real, Spain*
[2]*Max Born Institute, Max Born Str. 2a D-12489, Berlin, Germany*
(Received 20 November 2015; published 14 March 2016)

The energy loss of argon ions in a target depends on their velocity and charge density. At the energies studied in this work, it depends mostly on the free and bound electrons in the target. Here the random-phase approximation is used for analyzing free electrons at any degeneracy. For the plasma-bound electrons, an interpolation between approximations for low and high energies is applied. The Brandt-Kitagawa (BK) model is employed to depict the projectile charge space distribution, and the stripping criterion of Kreussler *et al.* is used to determine its equilibrium charge state Q_{eq}. This latter criterion implies that the equilibrium charge state depends slightly on the electron density and temperature of the plasma. On the other hand, the effective charge Q_{eff} is obtained as the ratio between the energy loss of the argon ion and that of the proton for the same plasma conditions. This effective charge Q_{eff} is larger than the equilibrium charge state Q_{eq} due to the incorporation of the BK charge distribution. Though our charge-state estimations are not exactly the same as the experimental values, our energy loss agrees quite well with the experiments. It is noticed that the energy loss in plasmas is higher than that in the same cold target of about, ∼42–62.5% and increases with carbon plasma ionization. This confirms the well-known enhanced plasma stopping. It is also observed that only a small part of this energy loss enhancement is due to an increase of the argon charge state, namely only ∼2.2 and 5.1%, for the partially and the fully ionized plasma, respectively. The other contribution is connected with a better energy transfer to the free electrons at plasma state than to the bound electrons at solid state of about, ∼38.8–57.4%, where higher values correspond to a fully ionized carbon plasma.

DOI: 10.1103/PhysRevE.93.033204

I. INTRODUCTION

Energy loss of ions propagating in matter has been subject of research in recent decades. Specifically, energy loss in solids and gases has been studied and developed for almost a century, so there are numerous models that reproduce and explain adequately experimental data [1–4]. However, the interaction of charged particles with partially and fully ionized matter (plasma) is still not totally understood and there are so far only a few experimental data that support the theoretical predictions [5–12].

The energy loss of ions in plasmas is relevant for many applications in different fields of science from fast ignition inertial fusion to medical applications [13–15]. Therefore, a large number of laboratories are presently accomplishing experiments on the interaction of ion beams with ionized matter [16–21].

Experiments often carry out have following setup: A thin foil of solid material (i.e., carbon) is irradiated with a laser pulse so it becomes a hot dense plasma. Simultaneously, an ion beam is sent into the material in opposite direction (to the target rear side). The ions penetrate the rear side that is still cold (solid) and arrive subsequently the hot dense plasma part at the front side, which expands and cools, leading to density and temperature gradients. In order to study the energy loss of ions in plasmas generated by a laser, it is important to know the transition from solid to plasma state in the target, which depends on the type of material and the excitation energy used. There are numerous codes that simulate laser interaction with the target and subsequent hydrodynamic expansion [22–27]. A set of diagnostics is also necessary that enable us to measure the conditions of the target with respect to temperature and density during the interaction time, such as laser interferometry for measuring displacement of the free electron density and x-ray spectroscopy for determination of the temperature [28].

The energy loss of projectiles in plasmas differs in solids and from that in gases due to the specific properties of the plasma. In the plasma case, projectiles interact not only with neutral atoms and bound electrons but also with ions and free electrons. Experiments presented in the literature [5,11,29,30] have shown that the energy loss of ions in plasmas is higher than in cold matter mainly for two reasons: an increase of projectile charge state and a more efficient energy transfer with the free electrons of the plasma. In this paper we focus on analyzing the first reason for the increase of energy loss, the increase of the projectile charge state.

Then, when calculating energy loss, an important aspect is to know the projectile charge state. There are various processes that modify the projectile charge state when it travels through the target. As it is impossible to measure this parameter for any projectile at any position during its propagation, it has to be determined theoretically. Whereas the charge state of the projectile principally increases when it loses electrons by collisions with target ions, it decreases due to the capture of the electrons bound to ions (recombination). There are also other effects that can change the charge state of the projectiles, but these two are the most dominant mechanisms. Finally, an equilibrium charge state is reached if the distance projectile traverse through the target is long enough. This equilibrium charge state is mainly a function of the projectile velocity [3,31–34].

Projectile charge state traversing fully ionized plasmas was first studied by Nardi and Zinamon [35], who showed

theoretically that the charge state is significantly higher than when they pass through cold matter. Later, this effect was experimentally verified [11,30,36,37]. This increase is mainly due to the reduction in the recombination processes of the projectile. This is caused by the smaller number of bound electrons in plasmas, which are captured by the projectiles as in case of a solid or a gas (direct free electron capture from a moving projectile violates a simultaneous conservation of energy and momentum). Charge-state enhancement affects the value of the energy deposited in the target, resulting in an increase of the energy loss in plasmas compared with cold matter.

In this work, the charge state and the energy loss of argon projectiles will be analyzed when traveling through two different ionized carbon plasmas, a partially and fully ionized one. This energy loss at the projectile velocities is due to the stopping with the free, mainly, and bound electrons of the plasma target. The contribution due to free electrons will be calculated through a dielectric formalism. The target (plasma) will be characterized by its dielectric function in the random-phase approximation (RPA) (Sec. II A). The contribution due to bound electrons will be obtained from an interpolation between an approximation for low and high energies (Sec. II B).

Regarding the description of the projectile (Sec. III A), as it is multielectronic, the model of Brandt-Kitagawa (BK) will be used, where the projectile electron density is set by a generic orbital which depends on a variational parameter. To define the equilibrium charge state of a heavy projectile, a method will be developed where the number of electrons bound to the projectile depends on the relative velocity between the projectile and the target electrons. The target electrons velocity will be defined by a function of the Fermi velocity (as in solids) plus a thermal velocity; and then the influence of the plasma properties on the charge state of the projectile will be studied. Both the increase in temperature and in electron density of the plasma contribute to an increase in the charge state, since these two effects lead to an increase of the target electron velocity and hence a reduction of the relative velocity. By decreasing this relative velocity, the number of electrons bound to the projectile core will be reduced, i.e., increasing its charge state.

Atomic units (a.u.), $e = \hbar = m_e = 1$, are used through all the work, unless other units are stated.

II. STOPPING POWER

A. Free electrons

The main reason of the energy loss for a projectile at high energies is the stopping caused by target electrons. Many models have been dedicated to calculate the electronic stopping power of different targets. One of the most common is the dielectric formalism introduced by Fermi [38] and further developed by Fermi and Teller [39].

In the dielectric formalism, the electron response of an isotropic and homogeneous material to a perturbation produced by an external charge density, $\rho_{\rm ext}(\mathbf{r},t)$, is contained in the dielectric function (DF), $\epsilon(\mathbf{r},t)$, of the medium. In this formalism, the expression to calculate the electronic stopping is well known [40], in a.u.,

$$S_{\rm fe}(v) = \frac{2}{\pi v^2} \times \int_0^\infty \frac{d\mathbf{k}}{k} \int_0^{kv} dw\, w\, [\rho_{\rm ext}(\mathbf{k},w)]^2 {\rm Im}\left[\frac{-1}{\epsilon(\mathbf{k},w)}\right], \quad (1)$$

where $\rho_{\rm ext}(\mathbf{k},w)$ and $\epsilon(\mathbf{k},w)$ are Fourier transforms of the projectile charge density and the target dielectric function, respectively.

The DF, $\epsilon(\mathbf{r},t)$, of a free electron gas without considering collisions between the target electrons, was calculated first by Lindhard [41] in the RPA. The RPA is usually valid at high projectile energies and when these electron collisions are not significant in the gas [42]. But as we here consider all kinds of plasmas, one has also these collisions to be taken into account. Recently, a new DF which includes these collisions for plasmas at any degeneracy has been obtained [43]. Differences in energy loss were only around 2% for plasmas with very high collision frequencies [44]. Then, in this work, RPA DF will be used for simplicity's sake.

RPA DF is developed in terms of the wave number $\mathbf{k}$ and of the frequency w provided by a consistent quantum mechanical analysis,

$$\epsilon(\mathbf{k},w) = 1 + \frac{1}{\pi^2 k^2} \int d^3k' \frac{f(\mathbf{k}+\mathbf{k}') - f(\mathbf{k}')}{w + i\upsilon - (E_{\mathbf{k}+\mathbf{k}'} - E_{\mathbf{k}'})}, \quad (2)$$

where $E_{\mathbf{k}} = k^2/2$. The temperature dependence is included through the Fermi-Dirac function

$$f(\mathbf{k}) = \frac{1}{1 + \exp[\beta(E_{\mathbf{k}} - \mu)]}, \quad (3)$$

where $\beta = 1/k_B T$ and μ the chemical potential of the plasma with the free electron density $n_{\rm fe}$ and the temperature T. As electron collisions are not considered in the RPA DF, the collision frequency approaches zero, $\upsilon \to 0$.

An analytic RPA DF for plasmas at any degeneracy can be obtained directly from Eq. (2) [45,46],

$$\epsilon_{\rm RPA}(k,w) = 1 + \frac{1}{4z^3 \pi k_F}[g(u+z) - g(u-z)], \quad (4)$$

where $g(x)$ corresponds to

$$g(x) = \int_0^\infty \frac{y dy}{\exp(Dy^2 - \beta\mu) + 1} \ln\left(\frac{x+y}{x-y}\right), \quad (5)$$

where $u = w/kv_F$ and $z = k/2k_F$ are the common dimensionless variables [41]. $D = E_F\beta$ is the degeneracy parameter and $v_F = k_F = \sqrt{2E_F}$ is Fermi velocity in a.u.

According to the Eq. (1), the electronic stopping of the projectile depends on its velocity and the Fourier transform of its charge density $\rho_{\rm ext}(\mathbf{k},w)$ that will be estimated in the next sections.

B. Bound electrons

In partially ionized plasmas, the stopping power of the electrons still bound to the target plasma ions must be taken into account. For a plasma target with atomic density $n_{\rm at}$, the

projectile stopping due to bound electrons has the forms [47]

$$S_{\rm be} = \frac{(Z-N)^2 4\pi n_{\rm at}}{v^2} L_{\rm be} \tag{6}$$

and

$$L_{\rm be} = \sum_i P_i L_i, \tag{7}$$

where Z is the atomic number of the projectile, N is the number of electrons bound to the nucleus, and $L_{\rm be}$ and L_i are the stopping number for whole electrons and each shell-bound electron of the target ion, respectively, and P_i is the average electron population in the shell of the target atom [48]. L_i is the reckoned interpolating between the asymptotic Bethe formulas valid either for low or for high projectile velocities [49]

$$L_i(v) = \begin{cases} L_{iH}(v) = \ln \frac{2v^2}{I_i} - \frac{2K_i}{v^2} & \text{for } v > v_{{\rm int}i} \\ L_{iB}(v) = \frac{\alpha_i v^3}{1+G_i v^2} & \text{for } v \leqslant v_{{\rm int}i} \end{cases}, \tag{8}$$

$$v_{{\rm int}i} = \sqrt{3K_i + 1.5 I_i}, \tag{9}$$

where G_i is given by $L_{iH}(v_{{\rm int}i}) = L_{iB}(v_{{\rm int}i})$.

Mean excitation energy, I_i, quantifies the energy exchanged in excitation and/or ionization processes of the electron shells. It is determined using

$$I_i = \sqrt{\frac{2K_i}{\langle r^2 \rangle_i}}, \tag{10}$$

where $\langle r^2 \rangle_i$ is the average of the square of the radius and K_i is the electron kinetic energy, for the electron in the i shell. The friction coefficient for low velocities of each shell is given within the hydrogenic approximation [50] by $\alpha_i = 1.067\sqrt{K_i}/I_i$.

Using Eq. (10), I_i can be easily estimated from the atomic parameters K_i and $\langle r^2 \rangle_i$. These parameters can be determined through several atomic methods like Hartree-Fock (HF) or oscillator strength (OS). The HF and OS methods have been already employed to calculate the stopping power of Xe, CH_2, LiH, and Al partially ionized plasmas, finding a very good agreement with experimental data [47,51].

III. PROJECTILE

A. Charge distribution

To calculate the electronic stopping of the projectile, it is necessary to know its charge. If the projectile is not considered pointlike, then the projectile charge density $\rho_{\rm ext}(\mathbf{r},t)$ can be regarded as a nucleus with a charge Z, which is pointlike, and an electron cloud with a charge density $\rho_{\rm e}(\mathbf{r},t)$ that will move with the velocity $\mathbf{v}$, provided that the relative velocity between the nucleus and the electron cloud is negligible. This is written as

$$\rho_{\rm ext}(\mathbf{r},t) = Z\,\delta(\mathbf{r}-\mathbf{v}t) - \rho_{\rm e}(\mathbf{r}-\mathbf{v}t), \tag{11}$$

and its Fourier transform is

$$\rho_{\rm ext}(\mathbf{k},w) = 2\pi\,\delta(w-\mathbf{k}\mathbf{v})[Z - \rho_{\rm e}(\mathbf{k})], \tag{12}$$

where $\rho_e(\mathbf{k})$ is the Fourier transform of the electron density of the projectile in an absolute value, because the minus sign in the equations above indicates the negative value of the electron charge. The BK model will be used to describe this electron charge distribution.

In the BK model [52], the density of electrons bound to the projectile is established by a generic orbital that depends on the variational parameter Λ,

$$\rho_{\rm eBK}(r) = \frac{N}{4\pi\Lambda^3}\frac{\Lambda}{r} e^{-\frac{r}{\Lambda}}, \tag{13}$$

where N is the number of electrons bound to the projectile, r is the distance to the nucleus, and Λ is

$$\Lambda(Z,N) = \frac{0.48 N^{2/3}}{Z - \frac{1}{7}N}. \tag{14}$$

The Fourier transform of the BK electron charge density needed in Eq. (1) is

$$\rho_{\rm eBK}(k) = \frac{N}{1+(k\Lambda)^2}. \tag{15}$$

B. Equilibrium charge state

If the projectile is considered pointlike, then as in most papers the definition of the equilibrium charge state, $Q_{\rm eq}$, is used in order to estimate the energy loss. The equilibrium charge state is the charge state that the ion projectile achieves after traveling inside the target till the electron capture and loss processes of the projectile are balanced. Our procedure to determine the equilibrium charge state of a projectile is based on the stripping criterion of Kreussler *et al.* [33]. They suggested that the equilibrium charge state of the projectile depends on the relative velocity of the projectile $\mathbf{v}$ to the electrons of the target $\mathbf{v}_e$, i.e., $v_r = |\mathbf{v} - \mathbf{v}_e|$. Considering all the possible orientations of vector $\mathbf{v} - \mathbf{v}_e$ gives

$$v_r = |\mathbf{v} - \mathbf{v}_e| = \frac{v_e^2}{6v}\left[\left(\frac{v}{v_e}+1\right)^3 - \left|\frac{v}{v_e}-1\right|^3\right]. \tag{16}$$

Kreussler has reported only on studies of solid materials and, therefore, only the valence electrons were considered for the calculation of the target electron velocity, $v_e = (2\frac{3}{5}E_{\rm F})^{1/2}$. In the case of a plasma, the target electron velocity is defined by its corresponding Fermi velocity, as for solids, plus a term due to temperature,

$$\begin{aligned} v_e &= \left(2\frac{3}{5}E_F + 3k_B T\right)^{1/2} = \left(\frac{3}{5}v_F^2 + 3v_{\rm the}^2\right)^{1/2} \\ &= \left(\frac{3}{5}\right)^{1/2} v_F \left(1 + \frac{5}{2}\theta\right)^{1/2}, \end{aligned} \tag{17}$$

where T is the plasma temperature, $v_{\rm the} = \sqrt{k_B T}$ is the thermal velocity, k_B is the Boltzman constant, v_F, is the Fermi velocity $E_F = 1/2 v_F^2$ in a.u., and $\theta = k_B T/E_F = 2v_{\rm the}^2/v_F^2$ is the reduced plasma temperature. By substituting this expression into Eq. (16), the relative velocity between the projectile and the plasma electrons is obtained.

The equilibrium charge state is then calculated as

$$Q_{\rm eq} = Z - N_{\rm eq} = Z - Ze^{-v_r/Z^{2/3}}, \tag{18}$$

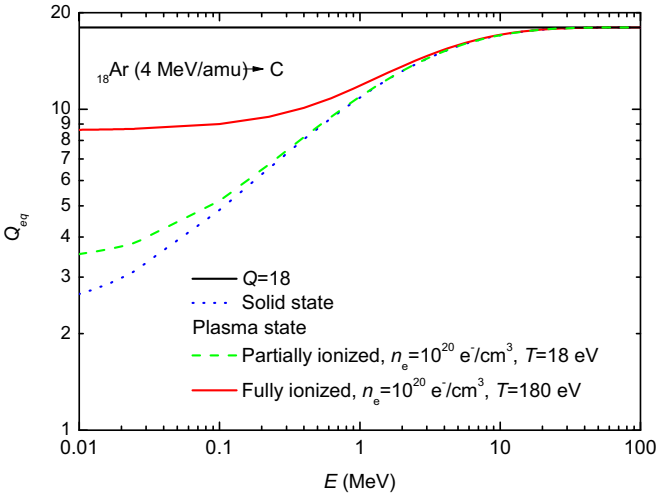

FIG. 1. Equilibrium charge state of argon projectiles ($Z = 18$) as a function of their energy, traveling through carbon at solid state or at different plasma states, partially or fully ionized.

where Z is the atomic number of the projectile, $N_{\rm eq}$ is the equilibrium number of bound electrons, and $Z^{2/3}$ is the velocity of the electrons bound to the projectile in the Thomas Fermi model (a.u.). The equilibrium charge state of the projectile increases together with its relative velocity, unless it achieves the limit value $Q_{\rm eq} = Z$ when the velocity is high enough.

Figure 1 shows the dependence of the equilibrium charge state of an argon projectile ($Z = 18$) on its velocity when traversing a solid or plasma carbon target. The differences between them are significant at low energies; the equilibrium charge state of the projectile is higher when it travels through the plasma, because the relative velocity in plasma also includes the thermal velocity of the electrons, see Eq. (17). The influence of the plasma conditions on the equilibrium charge state of argon ions can be also seen. When the plasma temperature increases, the equilibrium charge state of the projectile also increases, i.e., the number of electrons bound to the projectile is reduced. This effect is also more significant at low energies, because an increase of the plasma temperature implies an augmentation of the electron thermal velocity, Eq. (17) and thus a reduction in the relative velocity, Eq. (16) [40].

After obtaining the equilibrium number of electrons bound to the projectile $N_{\rm eq} = Ze^{-v_r/Z^{2/3}}$, it can be replaced in the BK electron charge distribution and also in the stopping formula, Eq. (1),

$$S_{\rm fe}(v) = \frac{2}{\pi v^2}\int_0^\infty \frac{dk}{k}\left[Z - \frac{N_{\rm eq}}{1+(k\Lambda)^2}\right]^2 \times \int_0^{kv} dw\, w\, {\rm Im}\left[\frac{-1}{\epsilon(k,w)}\right], \qquad (19)$$

where

$$\Lambda(v) = \frac{0.48 N_{\rm eq}^{2/3}}{Z - \frac{1}{7}N_{\rm eq}}.$$

IV. PARTIALLY IONIZED CARBON PLASMAS

Experimental data of energy loss of argon ions in a laser-generated carbon plasma have been reported in the paper [53]. It was shown that the argon ion loses its initial bound electrons but it simultaneously captures plasma electrons. In order to study the projectile charge state at any step inside the carbon plasma, Frank *et al.* [53] have used a Monte Carlo code. For this purpose, a code describing the evolution of the charge state of ions in cold matter, ETACHA [54], was extended to describe the special case of a plasma [55]. These codes use charge exchange cross sections for each projectile charge.

On the other hand, their theoretical description of the energy loss is to apply a modified version of the CASP code [56] that calculates the energy transferred from the projectile (with a defined charge state) to the free and bound electrons of the ionized carbon. The combination of the CASP code with the Monte Carlo calculation will be called MC CASP code. This allows for the determination of the electronic stopping of each projectile in its current charge state at each step when propagating through the target. In this model, a description of the equilibrium charge state of the projectile is not necessary.

The four experiments reported by Frank *et al.* [53] used Ar ions with an energy of 4 MeV/u ($v = 12.7$ a.u.). They investigated solid amorphous carbon foils with different line densities, $\delta = 90$, 94, 97, and 100 μg/cm^2, respectively, and a thickness of 0.5 μm, i.e., the volumetric density of this material is between 1.8 and 2 g/cm^3. In our case, the targets have an average value of the areal density of 95.3 μg/cm^2 $\pm$ 5%, so the volumetric density is $\rho = 95.3$ μg/cm^2/0.5 μm $=$ 1.91 g/cm^3 (it corresponds to an atomic density of $n_{\rm at} =$ 9.585×10^{22} at/cm^3 and a bound electron density of $n_{\rm be} =$ $6 \times n_{\rm at} = 5.75 \times 10^{23}$ e/cm^3).

In this case is the solid foil converted into a plasma state by irradiation with the nhelix laser system [53]. Figure 2 shows the carbon plasma conditions at the end of the laser pulse at 12 ns, when the ions traverse it. At this time, half of the plasma is fully ionized; the rest remains partially ionized (plasma ionization state, $q \approx 2$–4). Observing the region (40–80 μg/cm^2) in which the plasma is fully ionized ($q = 6$), one can recognize that the ion density decreases due to the plasma expansion. In Table I are given parameters for several points taken from

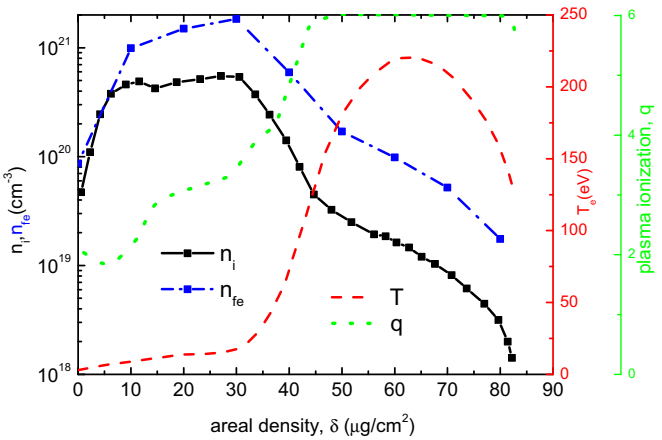

FIG. 2. Plasma parameters derived by the MC CASP code from Ref. [53], 12 ns after starting the laser pulse.

TABLE I. Plasma parameters derived from Fig. 2.

δ (μg/cm^2)	n_i (ions/cm^3)	ρ (g/cm^3)	l (cm)	T (eV)	q	n_{fe} (e/cm^3)
0	4.04×10^{19}	8.05×10^{-4}	0	2.76	2.14	8.65×10^{19}
10	4.7×10^{20}	9.37×10^{-3}	0.0011	9.18	2.11	9.92×10^{20}
20	4.89×10^{20}	9.74×10^{-3}	0.0021	13.54	3.06	1.50×10^{21}
30	5.38×10^{20}	1.07×10^{-2}	0.0028	17.92	3.41	1.83×10^{21}
40	1.23×10^{20}	2.45×10^{-3}	0.0163	72.97	4.82	5.93×10^{20}
50	2.83×10^{19}	5.64×10^{-4}	0.0896	179	6	1.70×10^{20}
60	1.64×10^{19}	3.27×10^{-4}	0.1836	219	6	9.84×10^{19}
70	8.66×10^{18}	1.73×10^{-4}	0.4056	210	6	5.20×10^{19}
80	2.92×10^{18}	5.82×10^{-5}	1.3749	156	6	1.75×10^{19}

the ion density distribution in the partially and fully ionized regions. For instance, the linear density of $\delta = 60$ μg/cm^2 corresponds to a density of $n_i = 1.64 \times 10^{19}$ ions/cm^3, which is equivalent to $\rho = 3.27 \times 10^{-4}$ g/cm^3. The corresponding free electron density at this point will be $n_{fe} = q \times n_i = 6 \times (1.6 \times 10^{19})$ ions/cm^3 $= 9.84 \times 10^{19}$ e/cm^3. This value is much less than the electron density calculated from the solid carbon density, $n_{be} = 5.75 \times 10^{23}$ e/cm^3, which is caused by the plasma volumetric expansion. The corresponding electron temperature at $\delta = 60$ μg/cm^2 is 219 eV.

A. Argon charge

In case of the argon projectiles, their charge state is one of the most relevant parameter to calculate the electronic stopping. The equilibrium charge state formula, Eq. (18) will be used in order to take into account the variability of their charge state depending on the conditions of plasma target. For instance, for an argon ion with an energy 4 MeV/u (velocity 12.7 a.u.) at the carbon plasma distance of 80 μg/cm^2, where the free electron plasma density is $n_{fe} = 1.752 \times 10^{19}$ e/cm^3, and the temperature is $T = 156$ eV, is the equilibrium charge state $Q_{eq} = Z - Ze^{-v_r/Z^{2/3}} = 15.35$. This result can be checked estimating the effective charge state from the electronic stopping, defined as

$$Q_{eff} \equiv \sqrt{S_{fe}(Ar)/S_{fe}(H^+)}, \tag{20}$$

evaluated at the same conditions as the last equilibrium charge state, Q_{eq}, i.e., at 80 μg/cm^2, $n_{fe} = 1.752 \times 10^{19}$ e/cm^3 and $T = 156$ eV. From Fig. 4 at 80 μg/cm^2, S_{fe}(Ar) $=$ 0.02069 eV/Å, and doing the same calculations for protons, $S_{fe}(H^+) = 8.613 \times 10^{-5}$ eV/Å. For this case is the effective charge state $Q_{eff} = 15.50$, which is approximately 1% higher than the equilibrium charge value, $Q_{eq} = 15.35$. This can be due to the use of the BK charge distribution, see Sec. III A, which causes an increase of the electronic stopping comparing with a pointlike charge distribution [40]. If we compare the plasma equilibrium charge state with those at solid carbon conditions, $n_e = 5.75 \times 10^{23}$ e/cm^3, one obtaines $Q_{eqs} = Z - Ze^{-v_r/Z^{2/3}} = 15.18$, which is slightly lower than the value for the last plasma state. As we do not calculate in this work the stopping power of the carbon solid, we cannot estimate the corresponding effective charge, Eq. (20). So the effective charge in solid is supposed to be about 1% higher than the equilibrium value, similary as in plasma state due to the BK distribution, resulting in a $Q_{effs} \simeq 15.33$.

Our results can be compared with those reported by Frank *et al.* [53] for different plasma conditions, see Fig. 3, showing a similar behavior: the charge state drop off in the partially ionized zone and increase in the fully ionized zone. According to their code MC CASP, the charge state of the projectile at 80 μg/cm^2 is $Q_{MCCASP} = 16.2$, i.e., higher than both the initial charge state of argon ions, $Q_0 = 16$, and the value they obtained for solids, $Q_{\text{MCCASPs}} = 15.6$. These calculations for the charge state from MC CASP code yielded quite higher values as compared with those from our model, even in the solid case. This can be checked comparing the results for solid carbon with the SRIM code for equilibrium charge state [3], $Q_{\text{eqSRIM}} = 14.73$. Using SRIM code, it is also possible to estimate the effective charge in solids, $Q_{\text{effSRIM}} = 14.87$, which is approximately 1% higher than the equilibrium value. It is surprising that the effective charge obtained with the SRIM code increases similar to our calculations. This fact, together with the fact that the SRIM results are closer to our values compared with those from the MC CASP code, confirms our results.

The point that our result for effective charge state in plasmas, $Q_{eff} = 15.50$, is a bit lower than the one obtained by the MC CASP code, $Q_{MCCASP} = 16.2$, can be due to the fact that the latter minimizes the effect of electron capture by the

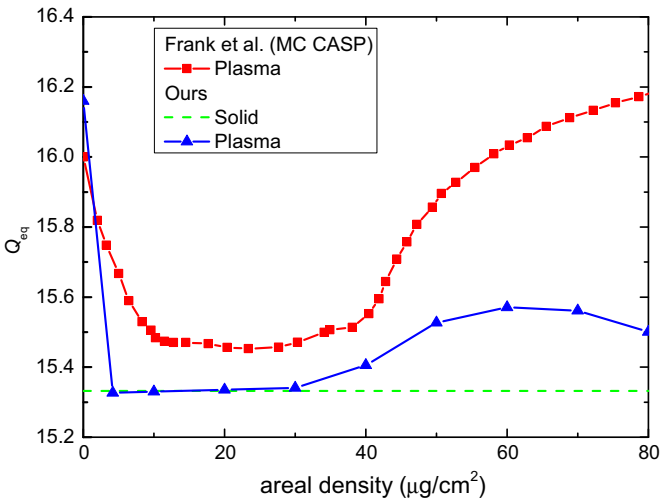

FIG. 3. Equilibrium charge state of argon ions traveling through the carbon plasma of Fig. 2. The red-square line was calculated with the MC CASP code from Ref. [53] and the blue-triangle line was calculated by us.

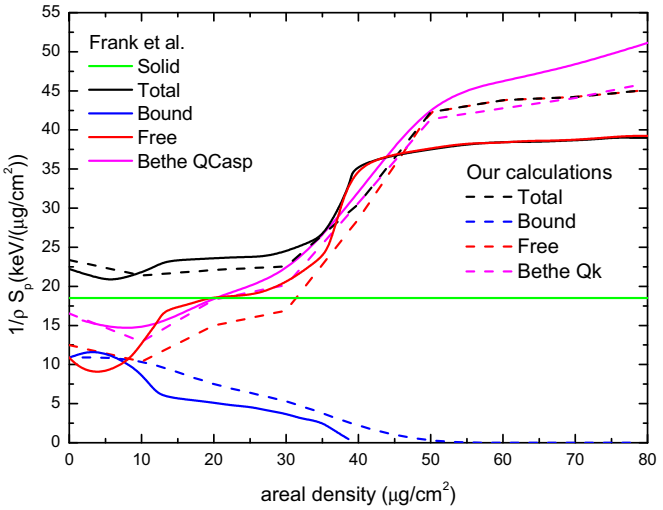

FIG. 4. Electronic stopping of Ar ions in carbon plasma calculated with MC CASP code [53] (solid lines) and with our model (dashed lines). SRIM data [3] for solid carbon and Bethe formula for free electrons are also plotted.

projectile, whereas the formula for the equilibrium charge state used in our model takes into account this effect in a similar way as for solids, $Q_{\text{effs}} = 15.33$. Another reason because the argon projectile does not reach the equilibrium charge state could be that the plasma is not large enough. The value of the final charge state will be normally higher than the equilibrium one, if the initial charge is higher than the equilibrium value. But in this work it is always supposed that the target is large enough so the projectile can achieve its equilibrium charge state. More surprising is the fact that our model with different charge estimations yields similar energy loss values as compared to those and experimentally shown in Ref. [53], see next section.

B. Argon energy loss

Next step to calculate argon projectile energy loss is to estimate its stopping with the target electrons. The electronic stopping estimated with the MC CASP code by Frank *et al.* [53] is plotted in Fig. 4. The figure shows the total electronic stopping (black solid line), the contribution of free (red solid line) and bound (blue solid line) plasma electrons calculated with the MC CASP code; additionally is also the solid carbon electronic stopping given (green solid line), with a constant value of 18.5 keV/(μg/cm^2). The results shows that in the coldest part of the plasma (partially ionized) both the bound and the free parts contribute to the total electronic stopping and the sum is only slightly higher than in the solid electronic stopping. However, in the fully ionized part the total electronic stopping is mostly caused by the free electron contribution and its value exceeds those for the solid case. This comes from the fact that energy transfer in the target is more efficient with free electrons, i.e., a fully ionized plasma is a medium with a high stopping power.

Our calculation results on electronic stopping are also added to the Fig. 4. For the solid carbon, we have used the SRIM code [3], $S_{\text{eSRIM}}(\text{Ar}, \rho = 1.91\ \text{g/cm}^3) = 353.3\ \text{eV/Å} \rightarrow 1/\rho \times S_{\text{eSRIM}} = 18.5\ \text{keV}/(\mu\text{g/cm}^2)$, the same as the value of Frank *et al.* [53]. In the following, is the electronic stopping in the carbon plasma 12 ns after the laser pulse estimated as shown in Fig. 2. For example, at $\delta = 60\ \mu\text{g/cm}^2$, where plasma parameters are $n_{\text{fe}} = 9.84 \times 10^{19}\ e/\text{cm}^3$ and $T = 219$ eV, is the free electronic stopping according to our theoretical model, Eq. (1), of $S_{\text{fe}}(\text{Ar}, n_e = 9.84 \times 10^{19}\ e/\text{cm}^3,\ T = 219\ \text{eV}) = 0.1432\ \text{eV/Å} \rightarrow 1/\rho \times S_{\text{fe}} = 43.82\ \text{keV}/(\mu\text{g/cm}^2)$. This value and other ones for the different line densities are depicted in Fig. 4 in the same colors but with dashed lines. Our results have similar behavior as those obtained from the code, showing an increasing with areal density, i.e., with degree of ionization. As it can be seen, our values are also a bit higher for the fully ionized part as compared to the values from their calculations. In their case is the difference with the value for a solid target of a factor of 2, whereas it is in our case a bit higher, 2.36. In order to find out what the best estimation is, the Fig. 4 shows also the results obtained with the well-known Bethe formula for high energies (as in this work, 4 MeV/u) considering only free electrons,

$$S_{\text{Befe}}(v) = \frac{Z^2 w_p^2}{v^2} \ln\left(\frac{2v^2}{w_p}\right), \tag{21}$$

where $w_p = \sqrt{4\pi n_{\text{fe}}}$ is the plasma frequency, all in a.u.. As it is seen, our results are more likely to the Bethe formula than to those obtained with the MC CASP code, such confirming our model. The Bethe QCasp and Qk results are obtained for plasma free electrons with the charge-state values from MC CASP code and also our model as given in Fig. 3. The QCasp results differ from their former estimation for high ionization degree in the plasma, whereas the Qk results agree quite well with our model. On the other hand, Eq. (6) is used to calculate the electronic stopping due to bound electrons. As it can be seen, our estimation has due to bound electrons the same tendency than the results from the MC CASP code.

Figure 5 shows the relative energy loss of argon ions in carbon foils heated by the laser pulses. According to the experimental data (blue up-triangles), one can state that as soon as the laser reaches the carbon foil, at 0 ns, a reduction of

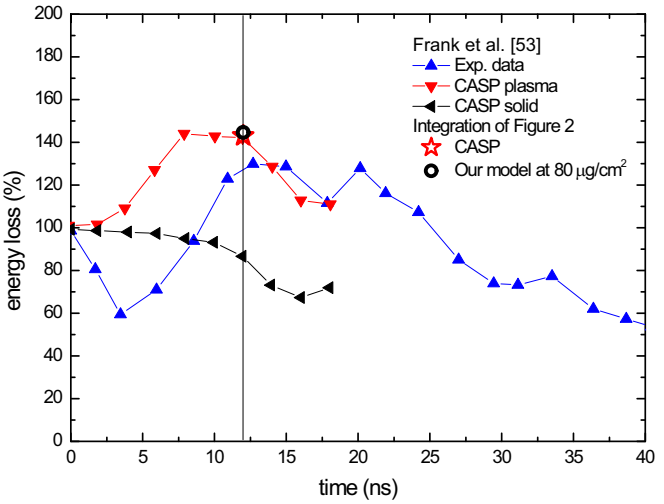

FIG. 5. Experimental and theoretical energy loss of Ar ions in carbon plasma.

the energy loss occurs, reaching a minimum value at 3–4 ns. Subsequently it grows and an energy loss value in solid carbon of 100% ≈ 1.8 MeV is achieved at 9 ns, reaching the maximum value at 13 ns (130% ≈ 2.35 MeV). The reason why the initial reduction in electronic stopping occurs is still unresolved, although it seems to be related to the possible inhomogeneities of the foil structure [53]. Anyway, to compare the experimental data with the theoretical results, we are mainly interested in the energy loss at 12 ns, since it is at this moment when we know the plasma parameters, see Fig. 2.

Results of calculations using MC CASP code are also included in the Fig. 5. It is clearly seen the difference between the results from theoretical code (red down-triangle) and the experimental data (blue up-triangles). Electronic stopping calculated with this code, assuming that the target is a neutral gas that expands with the same density distribution as the plasma, is also plotted (black left-triangle). One can recognize that their experimental as well as theoretical data (MC CASP code) for plasmas agree well for the interval between 12 and 18 ns after the laser pulse. In this period, more than half of the target is fully ionized, which explains the significant increase regarding cold matter of the electronic stopping due to free electrons.

In this Fig. 5 is the energy loss represented in percentages, where 100% corresponds to the energy loss in solid carbon, which is according to the data of Fig. 4 of 1.8 MeV. Twelve nanoseconds after the laser pulse is the value of the experimental energy loss of 127%, which corresponds to 2.29 MeV, whereas the MC CASP code calculation results in 140%, i.e., 2.52 MeV, which means the relative error is 13%.

To calculate the energy loss with our model, it is necessary to multiply the estimation of the stopping by the distance the projectile traveled in the target. For the solid, the distance is the thickness of the foil, 0.5 μm, leading to an energy loss of $\Delta E = S_{\mathrm{eSRIM}} \times \Delta x = 353.3\,\mathrm{eV/\AA} \times 0.5 \times 10^4\,\mathrm{\AA} = 1.8\,\mathrm{MeV}$, as in Frank *et al.* [53]. In case of the plasma state the distance is not the thickness of the solid carbon foil since simultaneously is the solid converted into plasma which expands conserving the number of ions. Therefore here, it is required to take into account the plasma areal density in its different states, i.e., the partially and the fully ionized parts. The energy loss in the plasma is estimated by integrating the values from Fig. 4 along areal density. Doing that for the total electronic stopping with the MC CASP code, one obtains approximately the same value as mentioned before, namely 2.53 MeV. On the other hand, the total energy loss estimated with our model is 2.56 MeV, which is exactly 142% of the energy loss in solid carbon. This result is similar to their theoretical calculation but a bit higher than the experimental result at 12 ns as shown in Fig. 5, $\Delta E_{\mathrm{Exp}} = 127\% \times 1.8\ \mathrm{MeV} = 2.29\ \mathrm{MeV}$. A reason for the difference could be that their estimations using the hydrodynamical code MIMOZA for plasma conditions at 12 ns were inaccurate. If the plasma electron density would be slightly smaller or the plasma temperature slightly higher, then the calculated energy loss will be lower, better approaching the experimental value.

To conclude, the energy loss calculated with our methods for the carbon plasma at 12 ns is 142% of the energy loss in solid carbon, which is a value similar to that obtained with the MC CASP code by Frank *et al.* [53], 140%, even though our model gives different charge-state values compared with their code as depicted in Fig. 3. It is notable that both theoretical estimations are a bit higher than the experimental results, 127%, which could be due to the fact that their estimations on the plasma conditions at 12 ns were inaccurate. Additionally, our results for stopping power coincide better with the results of the well-known Bethe formula at high energies, which also supports the correctness of our theoretical model.

This energy loss enhancement is analyzed in terms of an increase of the effective charge state of the projectile. Our model gives a charge state increase of 1.1%, which corresponds to a 2.2% surplus in the energy loss. However, this increase is not large enough to explain the gain in the total energy loss. It is supposed that the rest, ∼39.8%, will be due to a more efficient energy transfer with the free electrons of the plasma.

V. FULLY IONIZED CARBON PLASMAS

As mentioned in the Introduction, experiments in the literature show that the energy loss of ions in plasmas is higher than the energy loss in cold matter mainly for two reasons: an increase of projectile charge state and a more efficient energy transfer with the free electrons of the plasma. Following a new experiment of Frank *et al.* [57], where a fully ionized plasma has been achieved, we can now focus on analyzing the increase of the projectile charge state, neglecting the influence of the target ionicity. In a plasma, the cross sections for ionization and recombination of the projectile lead to different projectile charge states than in the solid, directly affecting its electronic stopping.

In the experiment the plasma was created by two laser beams irradiating a thin carbon foil of 0.5 μm from opposite sides, resulting in a fully ionized plasma of $n_e \simeq 10^{20}\ e/\mathrm{cm}^3$ and $T \simeq 180$ eV. Then an argon ion beam with an energy of 4 MeV/u ($v = 12.7$ a.u.) penetrates the target plasma. The diameter of the ion beam is reduced by a small pinhole to 500 μm. This assures that the ion beam interacts only with the central and most homogeneous part of the plasma of the same areal density.

A. Argon charge

The experimental charge state of argon ions evolves as follows (see Fig. 6): For times earlier than 0 ns, a constant mean charge state of 15.8 measured is for the solid target, which is 0.2 times higher than values reported in Ref. [53]; and more than once higher than the expectation from the SRIM code, $Q_{\mathrm{eqSRIM}} = 14.73$, see Sec. IV A. However, due to the nature of the plasma expansion, the target density decreases to $n_e = 10^{20}\ \mathrm{cm}^3$ after – ns. For this period, the charge state due to the interaction of the argon projectile with the plasma starts to exceed those in cold matter. The maximum mean charge state measured is 16.2 and hence 0.4 charge states higher than in solid target. The charge state in a gas compared to a solid foil is a bit lower [3,58], which is often called the density effect. This effect can be judged with the SRIM code [3] which gives $Q_{\mathrm{eqSRIMg}} = 14.69$, which is a bit smaller but does not significantly differ from the value for the solid, and therefore this density effect can be neglected. Thus, the experimental increase of the equilibrium charge state of the projectile due to the plasma transformation can be established as $\Delta Q_{\mathrm{exp}} \simeq$

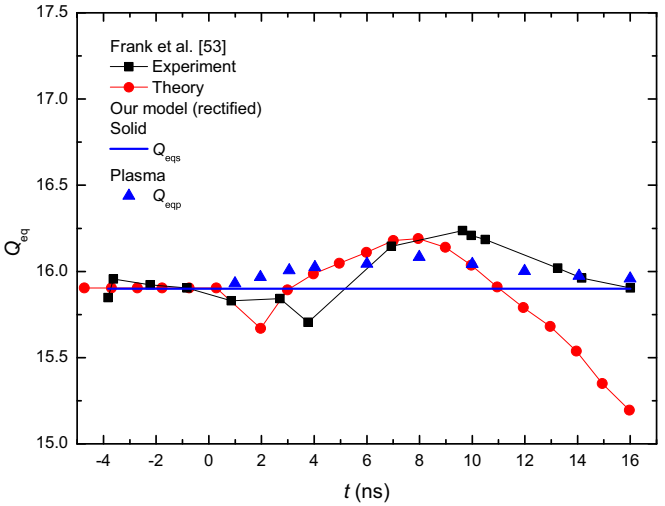

FIG. 6. Evolution of the equilibrium charge state of argon ions traversing the fully ionized carbon plasma.

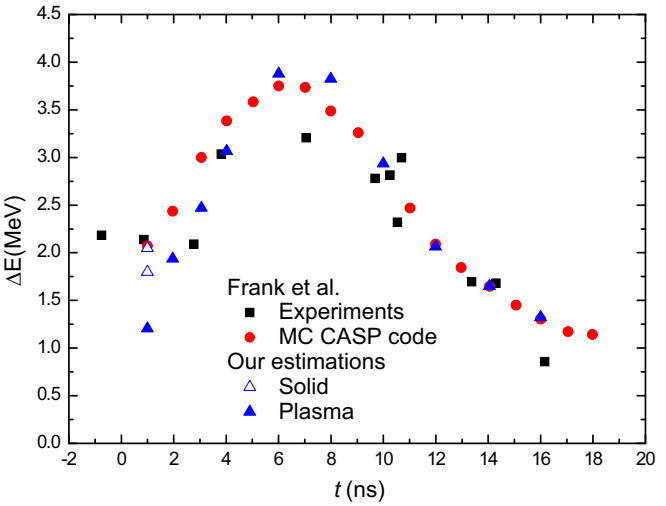

FIG. 7. Energy loss of argon ions at 4 MeV/u traversing the fully ionized carbon plasma.

0.4 or 2.5%, which is significant, since this corresponds to a change in the energy loss of 5.1%. But this is not the main reason for the total increase in the energy loss, as will be seen later.

For our model, the equilibrium charge state of argon ions at these plasma conditions ($n_e \simeq 10^{20}\ e/\text{cm}^3$ and $T \simeq 180$ eV) is $Q_{\text{eq}} = 15.37$, whereas the effective charge, Eq. (20), is $Q_{\text{eff}} = 15.52$, which is still far from the experimental datum of 16.2. The equilibrium charge state at solid carbon conditions ($n_{\text{e}} = 5.75 \times 10^{23}\ e/\text{cm}^3$) is $Q_{\text{eqs}} = 15.18$, and the effective charge $Q_{\text{effs}} = 15.33$, which is quite lower than their value for the solid of 15.8 but near the SRIM code with $Q_{\text{eqSRIM}} = 14.73$. Assuming the experimental data for the charge states are correct, the difference to our model could be explained with a mistake in calculating the plasma conditions by their code MIMOZA or by a difference in the incident energy of the projectile. For example, if the initial projectile energy is higher, then the charge state of the projectile in the targets also will be higher. As mentioned before, another reason could be that the argon projectile does not attain the equilibrium charge state if the target is not large enough, resulting in a final charge higher than the equilibrium one. This holds, of course, if the initial charge is higher than the equilibrium one. But in this work it is always supposed that the projectile achieves its equilibrium charge state.

For this case a shift in the value of our solid charge state is proposed in order to fit their experimental data for a solid (15.8) [57]. In the result, our estimations for the plasma state coincide quite well with the ones from experiments. In Fig. 6 shows values to compare our rectified model with their experimental and theoretical data depending on the plasma conditions at each time.

B. Argon energy loss

The energy loss of argon ions in solid carbon can be easily estimated multiplying the electronic stopping calculated before with the solid foil length of 0.5 μm. For the equilibrium charge state estimated by the SRIM code, $Q_{\text{eqSRIM}} = 14.73$, the energy loss is $\Delta E = S_{\text{eSRIM}} \times \Delta x = 353.3\,\text{eV/Å} \times (0.5 \times 10^4)$ Å $= 1.8$ MeV. This value is a bit lower than the experimental data, see Fig. 7, but equal to those obtained in the latter Sec. IV, and therefore one can conclude that one of them seems to be wrong. If the value of Frank *et al.* [57] for the charge state, 15.8, is used, then the energy loss now will be $\Delta E = S_{\text{eSRIM}} \times \Delta x = 409.4\,\text{eV/Å} \times (0.5 \times 10^4)$ Å $= 2.05$ MeV, which fits wellwith the experimental data for the solid state at short times, see Fig. 7.

For larger times, a plasma state is formed, resulting in an increase of the argon energy loss. This is the so-called EPS. In addition to the experimental data, Fig. 7 shows the estimation performed with their MC CASP code. From the figure, one can clearly recognize that, for shorter times, after 4 ns, their theoretical results (MC CASP code) are quite higher than the experimental values, while our calculations fit very well. At the maximum values, around 7 ns, there is not enough experimental information, but both their code and our estimations yield similar values of ~3.8 MeV, which is higher than the unique experimental value of 3.2 MeV. For the intermediate times, between 10 and 14 ns, their code and our model agree very well with the experimental data. For the last point measured, the theoretical estimations are over the experimental datum.

The EPS is supposed to be achieved in the time interval from 4 to 10 ns. In this interval, the difference between the experimental energy loss in cold and in the plasma state is approximately 46.7%, whereas the theoretical estimations gave about 62.5%. Moreover, the relative error between the experimental data and the theoretical models in calculating the EPS is about 15.8%, which is near the error values obtained for partially ionized carbon plasmas, 13–15%.

On the other hand, one has to remark that only a small part of the energy loss increase of 5.1% is due to the effect of the charge increase (as it is seen in last section), whereas the major part is caused by the more efficient energy transfer with the free electrons, ~57.4%. This contribution is higher than those corresponding to a partially ionized plasma of ~32.2%,

see Sec. IV B, because there are more free electrons in a fully ionized plasma. This confirms that most of the EPS is due to the transition from bound electrons in a solid state to free electrons in a plasma state.

VI. CONCLUSIONS

The energy loss of atomic projectiles in plasmas have been calculated with the models described above and compared with experimental data from the literature. Specifically, our calculations have been compared with the experimental data of argon projectiles with energy of 4 MeV/u propagating through a partially ionized carbon plasma [53]. Calculated energy loss values are somewhat higher, 142%, than the experimentally obtained one of 127%. Our value is similar to the value estimated for plasma conditions investigated with the MC CASP code from Ref. [53] of 140%. This could be due to the fact that the hydrodynamical code MIMOZA used by Frank *et al.* [53] yields plasma conditions that differ from the real ones. Using in the theoretical models reduced values of plasma electron density, which agrees with an expansion of the plasma, the energy loss would also be lower. Or if real plasma temperatures were higher than those obtained using their code, the theoretical energy loss will be lower than those in the experiments. Another reason could be that the initial projectile energy was higher than the one employed in the calculations, which also results in a small energy loss. Both the experimental data and values from the theoretical models indicate a considerable increase of the energy loss in plasmas compared to the one in solids of 100%, which is known as EPS.

The EPS has been analyzed in terms of an increase of the effective charge state of the projectile in the plasma target. Our model gives an equilibrium charge state increase of 1.1%, which is lower than the increase obtained by the code of Frank *et al.* Surprisingly, different estimations of the increase of the charge state gave similar results for the energy loss. An enhancement of 1.1% in the equilibrium charge state corresponds to an increase in the energy loss of 2.2%, which is only a small part of the total energy growth of ∼42%, and therefore it is supposed that the rest, ∼39.8%, will be caused by a more efficient energy transfer with the free electrons of the plasma.

To avoid the influence of the plasma ionization in any calculation, the energy loss of argon ions is also analyzed for a fully ionized carbon plasma of $n_e \simeq 10^{20}$ e/cm^3 and $T \simeq 180$ eV [57]. The charge state in solids calculated with our model is 15.33, which is again lower than the calculated one in the work of Frank *et al.* [57] of 15.8. Our value is more similar to the SRIM code experimental data. This could mean that the experiments have been done using initial projectile energies or target conditions that differ from those applied in the theoretical models. To solve this, our model was modified to fit the Frank *et al.* experimental value for a solid target. In this case our results for the fully ionized plasma were also similar to their experiments. The increase of the argon charge state in the plasma state is about 2.5% depending on the plasma conditions, which means the increase in the energy loss in the plasma target is 5.1%, i.e., it is larger than the 2.2% obtained for the partially ionized plasma. This confirms that the projectile charge state rises with the ionization of the plasma.

The energy loss using the modified charge state value has adjusted quite well to the experimental data. The difference between the experimental energy loss in cold and in the plasma state, i.e., the EPS, is approximately 46.7%, while the theoretical estimations yield about 62.5%. Then the relative error between the experimental data and the theoretical models in calculating the EPS is about 15.8%, which is similar to the error obtained for partially ionized carbon plasmas, 13–15%. Only a small part of the energy loss increase of 5.1% is due to the effect of the charge increase, whereas the major part, ∼57.4%, corresponds to the more efficient energy transfer of the projectile with the free electrons. This contribution is higher than those of a partially ionized plasma of ∼39.8%, because there are more free electrons in a fully ionized state. This confirms again that most of the EPS is due to the transition from bound electrons in the solid conditions to free electrons in a plasma.

ACKNOWLEDGMENTS

This work was financed by the Ministerio de Ciencia e Inovación (under contract No. ENE2013-45661-C2-1P). M.D.B.-C. thanks W. Cayzac for fruitful discussions and data.

[1] J. Lindhard and M. Scharff, Phys. Rev. **124**, 128 (1961).
[2] L. C. Northcliffe and R. F. Schilling, At. Data Nucl. Data Tables **7**, 233 (1970).
[3] J. J. F. Ziegler, J. P. Biersack, and U. Littmark, *The Stopping and Range of Ions in Solids* (Pergamon Press, London, 1985).
[4] F. Hubert, R. Bimbot, and H. Gauvin, At. Data Nucl. Data Tables **46**, 1 (1990).
[5] D. Gardes *et al.*, Europhys. Lett. **7**, 701 (1988).
[6] C. Deutsch *et al.*, Nucl. Instrum. Methods A **278**, 38 (1989).
[7] D. H. H. Hoffmann, K. Weyrich, H. Wahl, D. Gardes, R. Bimbot, and C. Fleurier, Phys. Rev. A **42**, 2313 (1990).
[8] K. G. Dietrich, D. H. H. Hoffmann, E. Boggasch, J. Jacoby, H. Wahl, M. Elfers, C. R. Haas, V. P. Dubenkov, and A. A. Golubev, Phys. Rev. Lett. **69**, 3623 (1992).
[9] P. Sigmund and A. Narmann, Laser Part. Beams **13**, 281 (1995).
[10] C. Stockl *et al.*, Laser Part. Beams **14**, 561 (1996).
[11] M. Kojima, M. Mitomo, T. Sasaki, J. Hasegawa, and M. Ogawa, Laser Part. Beams **20**, 475 (2002).
[12] E. Nardi, Y. Maron, and D. H. H. Hoffmann, Laser Part. Beams **25**, 489 (2007).
[13] S. Eliezer, M. Murakami, and J. M. M. Val, Laser Part. Beams **25**, 585 (2007).
[14] M. D. Barriga-Carrasco, Phys. Plasmas **15**, 033103 (2008).
[15] R. C. Cook *et al.*, Laser Part. Beams **26**, 479 (2008).
[16] P. K. Roy, S. S. Yu, E. Henestroza, A. Anders, F. M. Bieniosek, J. Coleman, S. Eylon, W. G. Greenway, M. Leitner, B. G. Logan, W. L. Waldron, D. R. Welch, C. Thoma, A. B. Sefkow, E. P.

Gilson, P. C. Efthimion, and R. C. Davidson, Phys. Rev. Lett. **95**, 234801 (2005).
[17] B. Y. Sharkov, N. N. Alexeev, M. M. Basko, M. D. Churazov, D. G. Koshkarev, S. A. Medin, Y. N. Orlov, and V. M. Suslin, Nucl. Fusion **45**, S291 (2005).
[18] Y. Oguri, K. Kashiwagi, J. Kaneko, J. Hasegawa, M. Yoshida, and M. Ogawa, Phys. Rev. ST Accel. Beams **8**, 060401 (2005).
[19] D. H. H. Hoffmann *et al.*, Laser Part. Beams **23**, 47 (2005).
[20] T. Someya, T. Kikuchi, K. Miyazawa, S. Kawata, and A. I. Ogoyski, J. Phys. IV **133**, 743 (2006).
[21] B. G. Logan, R. O. Bangerter, D. A. Callahan, M. Tabak, M. Roth, L. J. Perkins, and G. Caporaso, Fusion Sci. Technol. **49**, 399 (2006).
[22] Jon T. Larsen and Stephen M. Lane, J. Quant. Spectrosc. Radiat. Transfer **51**, 179 (1994).
[23] M. M. Marinak, R. E. Tipton, O. L. Landen, T. J. Murphy, P. Amendt, S. W. Haan, S. P. Hatchett, C. J. Keane, R. McEachern, and R. Wallace, Phys. Plasmas **3**, 2070 (1996).
[24] I. Sofronov *et al.*, Series Mathematical Modeling of Physical Processes **1**, 25 (2000).
[25] J. J. MacFarlane, I. E. Golovkin, R. C. Mancini, L. A. Welser, J. E. Bailey, J. A. Koch, T. A. Mehlhorn, G. A. Rochau, P. Wang, and P. Woodruff, Phys. Rev. E **72**, 066403 (2005).
[26] A. Tauschwitz, M. Basko, A. Frank, V. Novikov, A. Grushin, A. Blazevic, M. Roth, and J. A. Maruhn, High Energy Density Phys. **9**, 158 (2013).
[27] P. Tzeferacos, M. Fatenejad, N. Flocke, C. Graziani, G. Gregori, D. Q. Lamb, D. Lee, J. Meinecke, A. Scopatz, and K. Weide, High Energy Density Phys. **17**, 24 (2015).
[28] A. Blazevic, B. Rethfeld, and D. Hoffmann, K. Dan. Vidensk. Selsk. Mat. Fys. Medd. **52**, 109 (2006).
[29] K. Weyrich *et al.*, Nucl. Instrum. Methods A **278**, 52 (1989).
[30] A. Golubev *et al.*, Nucl. Instrum. Methods Phys. Res. Sect. A-Accel. Spectrom. Dect. Assoc. Equip. **464**, 247 (2001).
[31] A. Bohr, K. Dan. Vidensk. Selsk. Mat. Fys. Medd. **24**, 1 (1948).
[32] L. C. Northcliffe, Phys. Rev. **120**, 1744 (1960).
[33] S. Kreussler, C. Varelas, and W. Brandt, Phys. Rev. B **23**, 82 (1981).
[34] T. Peter and J. Meyer-ter-Vehn, Phys. Rev. A **43**, 2015 (1991).
[35] E. Nardi and Z. Zinamon, Phys. Rev. Lett. **49**, 1251 (1982).
[36] D. H. H. Hoffmann *et al.*, Nucl. Instrum. Methods B **90**, 1 (1994).
[37] E. Nardi, D. V. Fisher, M. Roth, A. Blazevic, and D. H. H. Hoffmann, Laser Part. Beams **24**, 131 (2006).
[38] E. Fermi, Phys. Rev. **57**, 485 (1940).
[39] E. Fermi and E. Teller, Phys. Rev. **72**, 399 (1947).
[40] M. D. Barriga-Carrasco, Phys. Rev. E **88**, 043107 (2013).
[41] J. Lindhard, K. Dan Vidensk. Selsk. Mat.-Fys. Medd. **28**, 1 (1954).
[42] C. Barnes and J. M. Luck, J. Phys. A: Math. Gen. **23**, 1717 (1990).
[43] M. D. Barriga-Carrasco, Phys. Rev. E **82**, 046403 (2010); Laser Part. Beams **28**, 307 (2010).
[44] M. D. Barriga-Carrasco, Laser Part. Beams **29**, 81 (2011).
[45] C. Gouedard and C. Deutsch, J. Math. Phys. **19**, 32 (1978).
[46] N. R. Arista and W. Brandt, Phys. Rev. A **29**, 1471 (1984).
[47] D. Casas, M. D. Barriga-Carrasco, and Juan Rubio, Phys. Rev. E **88**, 033102 (2013).
[48] M. D. Barriga-Carrasco and G. Maynard, Laser Part. Beams **23**, 211 (2005).
[49] G. Maynard and C. Deutsch, J. Physique **46**, 1113 (1986).
[50] X. Garbet, C. Deutsch, and G. Maynard, J. Appl. Phys. **61**, 907 (1987).
[51] M. D. Barriga-Carrasco and D. Casas, Laser Part. Beams **31**, 105 (2013).
[52] W. Brandt and M. Kitagawa, Phys. Rev. B **25**, 5631 (1982).
[53] Frank *et al.*, Phys. Rev. E **81**, 026401 (2010).
[54] J. P. Rozet *et al.*, Nucl. Instrum. Methods B **107**, 67 (1996).
[55] A. Blažević, H. G. Bohlen, and W. von Oertzen, Phys. Rev. A **61**, 032901 (2000).
[56] P. L. Grande and G. Schiwietz, Phys. Rev. A **58**, 3796 (1998).
[57] Frank *et al.*, Phys. Rev. Lett. **110**, 115001 (2013).
[58] N. E. B. Cowern, C. J. Woods, and C. J. Sofield, Nucl. Instrum. Methods **216**, 287 (1983).